

Anchoring Ligand Engineering Enables Highly Stable MA-Free Perovskite Solar Cells with a Minimal Voc Deficit of 0.32 V

Chaohui Li^{1,10*}, Andrej Vincze³, Hyoungwon Park⁴, Fabian Streller⁵, Klaus Götz⁶, Shudi Qiu¹, Jiwon Byun⁷, Ying Shang⁸, Zhangyu Yuan⁸, Lirong Dong¹, Jingjing Tian^{1,10}, Zijian Peng^{1,10}, Chao Liu^{1,2}, Fu Yang⁹, Yanxue Wang^{1,2}, Andreas Späth^{5,12}, Andres Osvet¹, Karen Forberich^{1,2}, Thomas Heumueller^{1,2}, Silke H. Christiansen^{4,11}, Marcus Halik⁷, Rainer H. Fink⁵, Tobias Unruh⁶, Ning Li⁸, Larry Lüer.^{1*}, and Christoph J. Brabec^{1,2*}

¹ Institute of Materials for Electronics and Energy Technology (i-MEET), Department of Materials Science and Engineering, Friedrich-Alexander-Universität Erlangen-Nürnberg, Martensstrasse 7, 91058 Erlangen, Germany

² Helmholtz-Institute Erlangen-Nürnberg for Renewable Energy (HI ERN), FAU Profile Center Solar, Immerwahrstrasse 2, 91058 Erlangen, Germany

³ International Laser Centre SCSTI, Ilkovičova 3, 84104 Bratislava, Slovak Republic

⁴ Fraunhofer Institute for Ceramic Technologies and Systems IKTS, Äußere Nürnberger Strasse 62, 91301 Forchheim, Germany

⁵ Physical Chemistry II and Interdisciplinary Center for Molecular Materials, Friedrich-Alexander-Universität Erlangen-Nürnberg, Egerlandstrasse 3, 91058 Erlangen, Germany

⁶ Institute for Crystallography and Structural Physics, Friedrich-Alexander-Universität Erlangen-Nürnberg, Staudtstrasse 3, 91058 Erlangen, Germany

⁷ Organic Materials and Devices, Department of Materials Science, Interdisciplinary Center for Nanostructured Films (IZNF), Friedrich-Alexander-Universität Erlangen-Nürnberg, 91058 Erlangen, Germany;

⁸ Institute of Polymer Optoelectronic Materials and Device, Guangdong Basic Research Center of Excellence for Energy and Information Polymer Materials, State Key Laboratory of Luminescent Materials and Devices, South China University of Technology, Guangzhou 510640, China

⁹ Laboratory of Advanced Optoelectronic Materials, Suzhou Key Laboratory of Novel Semiconductor-Optoelectronics Materials and Devices, College of Chemistry, Chemical Engineering and Materials Science, Soochow University, Suzhou, 215123, China

¹⁰ Erlangen Graduate School in Advanced Optical Technologies (SAOT) Paul-Gordan-Straße 6, 91052 Erlangen, Germany

¹¹ Freie Universität Berlin, Physics Department, Arnimallee 14, 14195 Berlin

¹² FAU Competence Center Engineering of Advanced Materials, Friedrich-Alexander-Universität Erlangen-Nürnberg, Cauerstrasse 3, 91058 Erlangen, Germany

*Correspondence: C. H. Li.: chaohui.li@fau.de; L. L.: larry.lueer@fau.de; C. J. B.: christoph.brabec@fau.de.

Experimental Section

Materials:

Lead iodide (PbI_2 , 99.99%), and [4-(3,6-Dimethyl-9H-carbazol-9-yl)butyl]phosphonic Acid (Me-4PACz) were purchased from TCI Development Co. Formamidinium iodide (FAI, $\geq 99.5\%$) and 4-Chlorophenethylammonium iodide (ClPEAI) were ordered from Greatcell Solar Ltd. Methylammonium bromide (MABr, $\geq 99.5\%$), Methylammonium chloride (MACl, $\geq 99.5\%$) was purchased from Xi'an polymer Light Technology Corp. Lead bromide (PbBr_2 , 99.999%), Cesium iodide (CsI, 99.9%), Methylphosphonic acid (MPA, 98%), Ethanol absolute (EtOH), dimethyl sulfoxide (DMSO, $\geq 99.9\%$), N, N-dimethylformamide (DMF, 99.8%), ethyl acetate (EA $\geq 97\%$), NiOx nanoparticles was obtained Advanced ElectionTechnology Co., Ltd. Ethanolamin ($\geq 99\%$), Ethanol($\geq 99.8\%$) and Al_2O_3 dispersion (30 nm, 20 wt% in isopropanol), chlorobenzene (CB, 99.8%), Triphenylphosphine oxide (TPPO, 98%) and Bathocuproine (BCP) were obtained from Sigma-Aldrich. Isopropanol ($\geq 99.9\%$) was purchased from Aladdin. PC₆₁BM was purchased from Nano-C. All the chemicals were used as received without further purification.

Preparation of control and target films and devices

The pre-patterned ITO-coated glass substrates ($25 \times 25 \text{ mm}^2$ with sheet resistance of 15 ohm/sq) were cleaned by ultrasonication in acetone and isopropanol for 10 min each. Before deposition, the bare ITO substrate was treated with UV-ozone for 10min. First, NiOx nanopartical (10 mg ml⁻¹ in H₂O) layer was spin coated on as-cleaned ITO substrates at 4000 rpm for 30 s, and then annealed at 150 °C for 10 min in ambient air, followed by immediately transfer into a nitrogen-

filled glove box. The hole transport layers of Me-4PACz and MPA were sequentially deposited on the ITO substrate at 4000 rpm for 30 s and annealed at 100 °C for 10 min, the concentration of precursor was 0.5 mg/mL of Me-4PACz or MPA in alcohol solution. The above processes were performed in the N₂-globlox. After that, Al₂O₃ nanoparticles were diluted in IPA (Al₂O₃/IPA=1:50, v:v), spin-coated onto the SAM layer at 5000 rpm for 30 seconds, and subsequently annealed at 100 °C for 5 minutes. the perovskite layer was deposited by using the one-step spin-coating method in the N₂-filled glovebox. 1.5 M FA_{0.9}Cs_{0.1}PbI₃ perovskite precursor was prepared by dissolving 232.2 mg FAI, 38.97 mg CsI, 25 mg MACl, 726 mg PbI₂ in conventional solvent system (DMF/DMSO= 5:1, v:v). The perovskite solution was deposited onto the above substrates at 1000 rpm for 5 s and 5000 rpm for 30 s, 280 μL EA was dripped onto the center of the film at 10 s before the end of program, followed by annealing on a hotplate at 110 °C for 30 min. Next, a mixture of 1 mg ClPEAI/MAI (2:1, wt/wt) was dissolved in 1 mL IPA–DMF (200:1, v/v), deposited onto the upper of perovskite films at 4000 rpm for 30 s and then annealed at 100 °C for 5 min. Subsequently, Then TPPO solution was deposited on the ClPEAI layer at 5000 rpm for 30 s and annealed at 85 °C for 5 min. PCBM (20 mg/mL) solution was spin-coated on the perovskite layer at 2000 rpm for 30 s and then annealed for 5 min at 70 °C. BCP (0.25 mg/mL) solution was deposited on the PCBM layer with 4000 rpm 30 s. Finally, the Ag electrode (100 nm) was evaporated on the BCP layer using the thermal evaporation method and the fixed active area of this electrode was 0.04 cm². Note that all solutions are filtered using a 0.22 μm Polytetrafluoroethylen (PTFE) filter before spin coating. For both FA_{0.82}MA_{0.13}Cs_{0.05}Pb(I_{0.87}Br_{0.13})₃ (bandgap ≈ 1.59 eV)- and

$\text{Cs}_{0.22}\text{FA}_{0.78}\text{PbI}_{1.8}\text{Br}_{1.2}$ (bandgap ≈ 1.797 eV)-bandgap perovskites, we employed the same fabrication process as that used for the 1.55 eV bandgap perovskite

Characterizations:

X-ray diffraction (XRD) measurement: The crystal structure was characterized by Panalytical X'pert powder diffractometer (XRD) with Cu K α radiation ($\lambda = 1.54178$ Å) and an X'Celerator solid-state stripe detector operated at 40 kV and 30 mA.

X-ray photoelectron spectroscopy (XPS) measurement: XPS were performed on an EA 125X U7 Energy Analyser from Scienta Omicron using Al K α radiation with 1486.7 eV excitation energy, 0.05 eV step with 20 eV pass and 5 s dwell was used for XPS analysis.

Scanning electron microscopy (SEM) images: The morphologies of the perovskite films were investigated by scanning electron microscope (JEOL JSM-7610F).

A double-beam spectrophotometer (Lambda 950, PerkinElmer) equipped with an integrated sphere was used for the UV-vis absorption measurement.

Photoluminescence (PL) spectra: PL was carried out using a steady-state spectroscope (FluoTime 300, PicoQuant GmbH) excited by a 402 nm laser.

Impedance spectra: The Mott-Schottky and Nyquist plots measurements were performed on an electrochemical workstation (ZAHNER, Germany). The impedance spectra and built-in potential (V_{bi}) were correspondingly measured in dark and under illumination with a LED lamp (LSW-2, s/n LS 1858).

Kelvin force microscope (KPFM) images: KPFM measurements were done with the NX10 (Park Systems), installed inside of the Ar-filled glovebox for the inert atmosphere measurement. PPP-EFM probe (resonance frequency of 75 kHz, Spring constant of 2.8 N m^{-1} , coated with PtIr5 on both sides) was used to obtain the $2 \times 2 \mu\text{m}^2$ area images, with a 512×512 pixel resolution.

Obtained data was processed with Park SmartAnalysis™ software.

Current density-voltage (*J*-*V*) measurement: *J*-*V* characteristics of the solar cells were measured using a Keithley 2400 source meter. The illumination was provided by a Newport Sol3A solar simulator with an AM1.5G filter, operating at 100 mW cm⁻², which was calibrated by a standard silicon solar cell from Newport. Both forward and backward scans were performed, and the scan rate of 20 ms/step and a scan step of 40 mv. The external quantum efficiency (EQE) of the perovskite solar cell device was measured by using a QE-R instrument from Enlitechnology.

Time-of-flight secondary ion mass spectrometry (TOF-SIMS) measurement: The SIMS depth profiles were acquired by using a Time-of-Flight SIMS IV (Ion-TOF GmbH, Muenster, Germany) equipped with a Bi⁺ primary ion gun working at 25 keV in dual beam mode under the UHV conditions. The sputtering was realized with Cs⁺ ion guns at 1 keV energy using of active electron flooding to prevent the surface charging to increase the yield of negatively charged secondary ions. While the sputtering Cs⁺ gun creating the crater, the primary ion beam with Bi⁺ is progressively analyzing the crater bottom. The usual configuration for depth profiles is to sputter 300 × 300 μm² from the sample surface and the analysis is then done in the middle of this area 84 × 84 μm². After a careful calibration using to known spectral lines, the data files were analyzed by SurfaceLab software provided by Ion-TOF. For the selected ions like I⁻ and Ag⁻ a peak list was created and then the depth profile evaluated. All samples were measured under same conditions.

Quasi-Fermi level spitting (QFLS) measurements: QFLS was calculated according to previous our group reports.¹⁻³ In this work, we calculate the QFLS according to

$$QFLS = QFLS_{rad} + k_B T \ln \left(\frac{J_G}{J_{0,rad}} \right)$$

$$QFLS_{rad} = kT \ln \left(\frac{J_G}{J_{0,rad}} \right)$$

where QFLS_{rad} is the QFLS in the radiative limit, J_G , $J_{0, \text{rad}}$, k and T are generation current density, dark radiative saturation current density, Boltzmann constant, thermal equilibrium temperature, respectively. J_G here is the integrated product of EQE spectra and $J_{0, \text{rad}}$ can be determined by:

$$J_{0,rad} = q \int E QE_{PV}(E) \phi_{bb}(E) dE$$

$$\phi_{bb}(E) = \frac{2\pi E^2}{(h^3 c^2)} \exp\left(-\frac{E}{kT}\right)$$

where q is the elementary charge, E the photo energy, h the Planck constant and c the light velocity in vacuum.

Long term stability measurement: Devices without encapsulation were loaded into a degradation chamber flowed with N₂-chamber Light source was provided by 4 white LED (XLamp® CMA3090 LED) without using filter. The light intensity was calibrated with a Si reference cell (91150V) bought from Newport. Temperature is controlled via hotplate and monitored at all times with a temperature detector (PT100). The J-V characteristics were measured by LabView program with different interval time (2-10 minutes in the early stages and 45-90 minutes in the later stages).

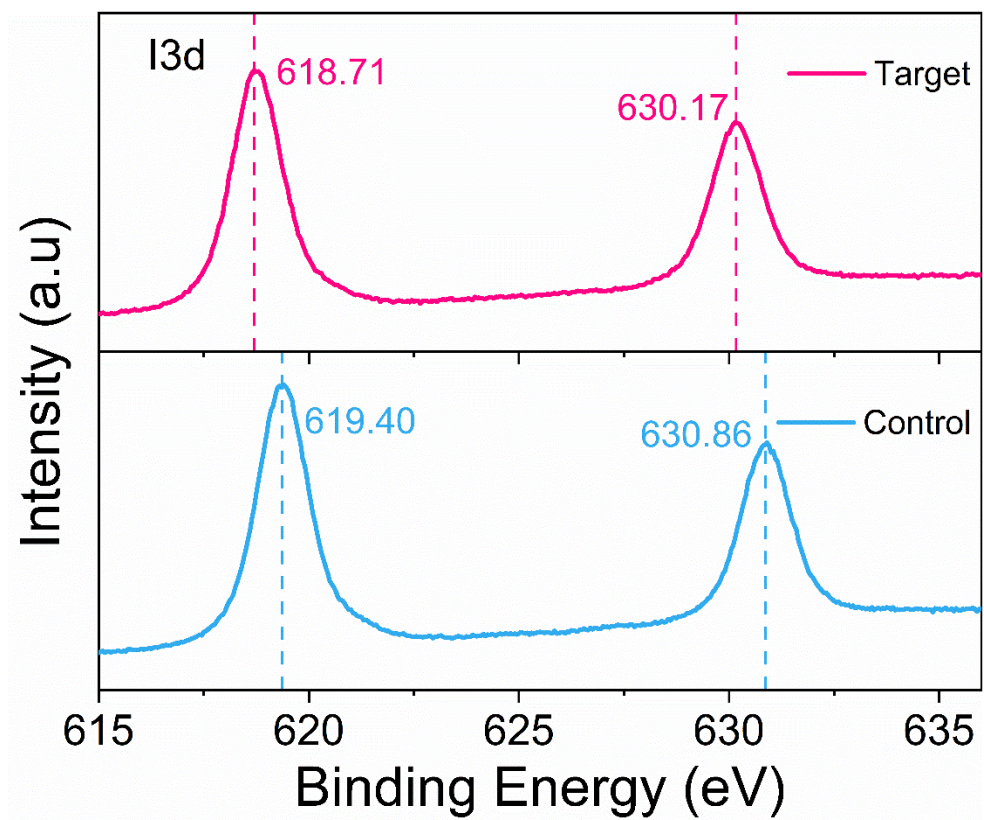


Figure S1 XPS spectra of I 3d peaks of perovskite surface control and modified by TPPO (Target).

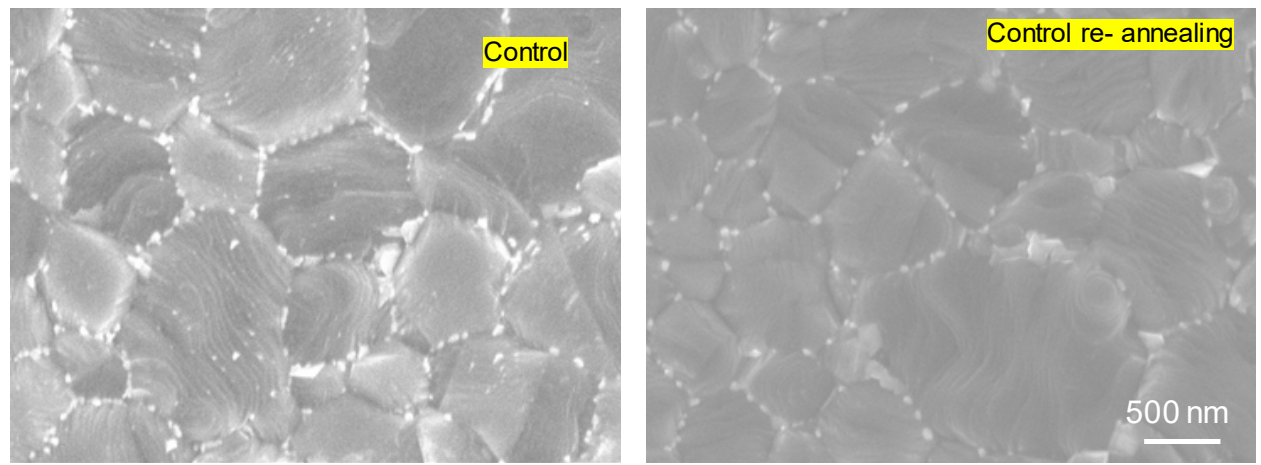


Figure S2 Top-view SEM images of the (a) control and (b) control re-annealing films, Sample structure: ITO/NiOx/SAM/Perovskite

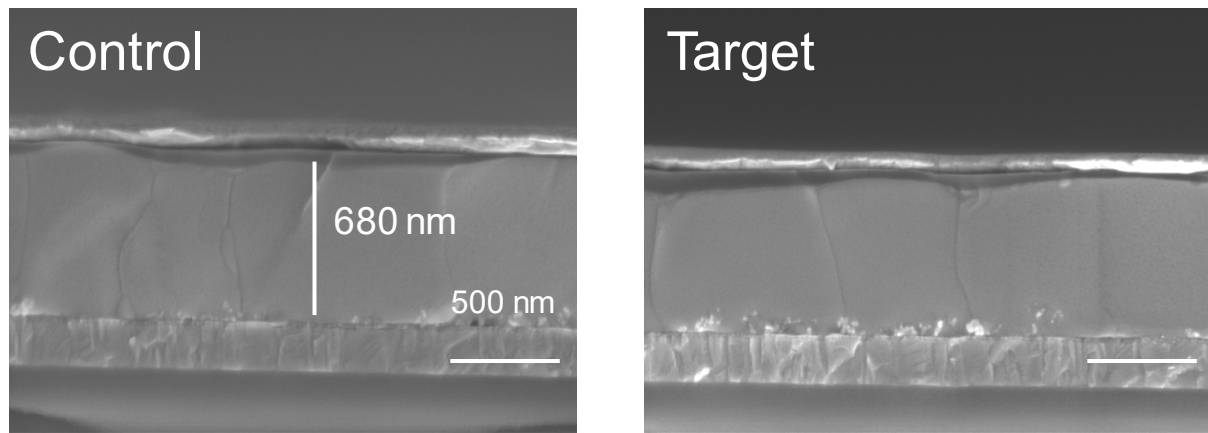


Figure S3 Cross-section SEM image of control and target PSCs, the structure of ITO/NiO@SAM/perovskite/TPPO (w/o.w)/PCBM/BCP/Ag.

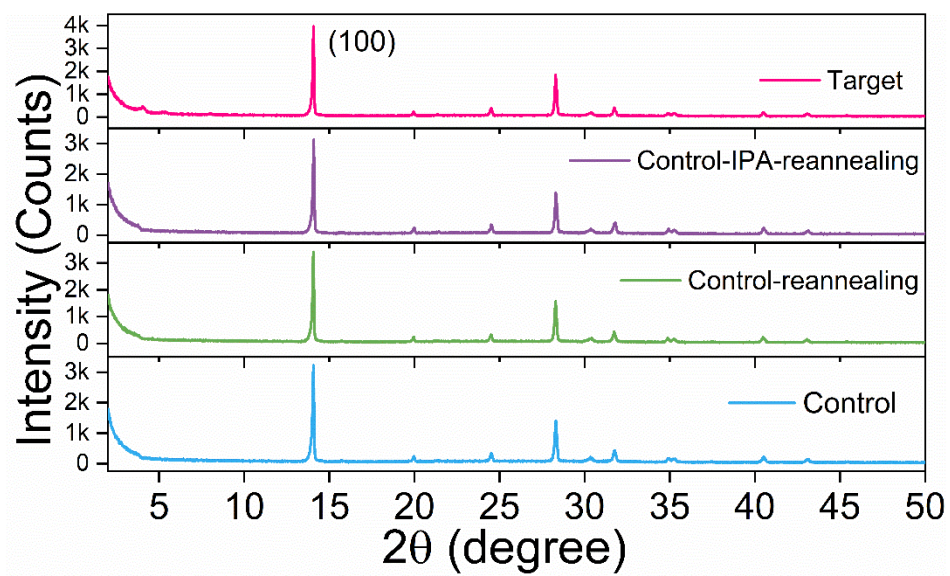


Figure S4 XRD image of control, Control re-annealing, Control@IPA re-annealing, Target samples

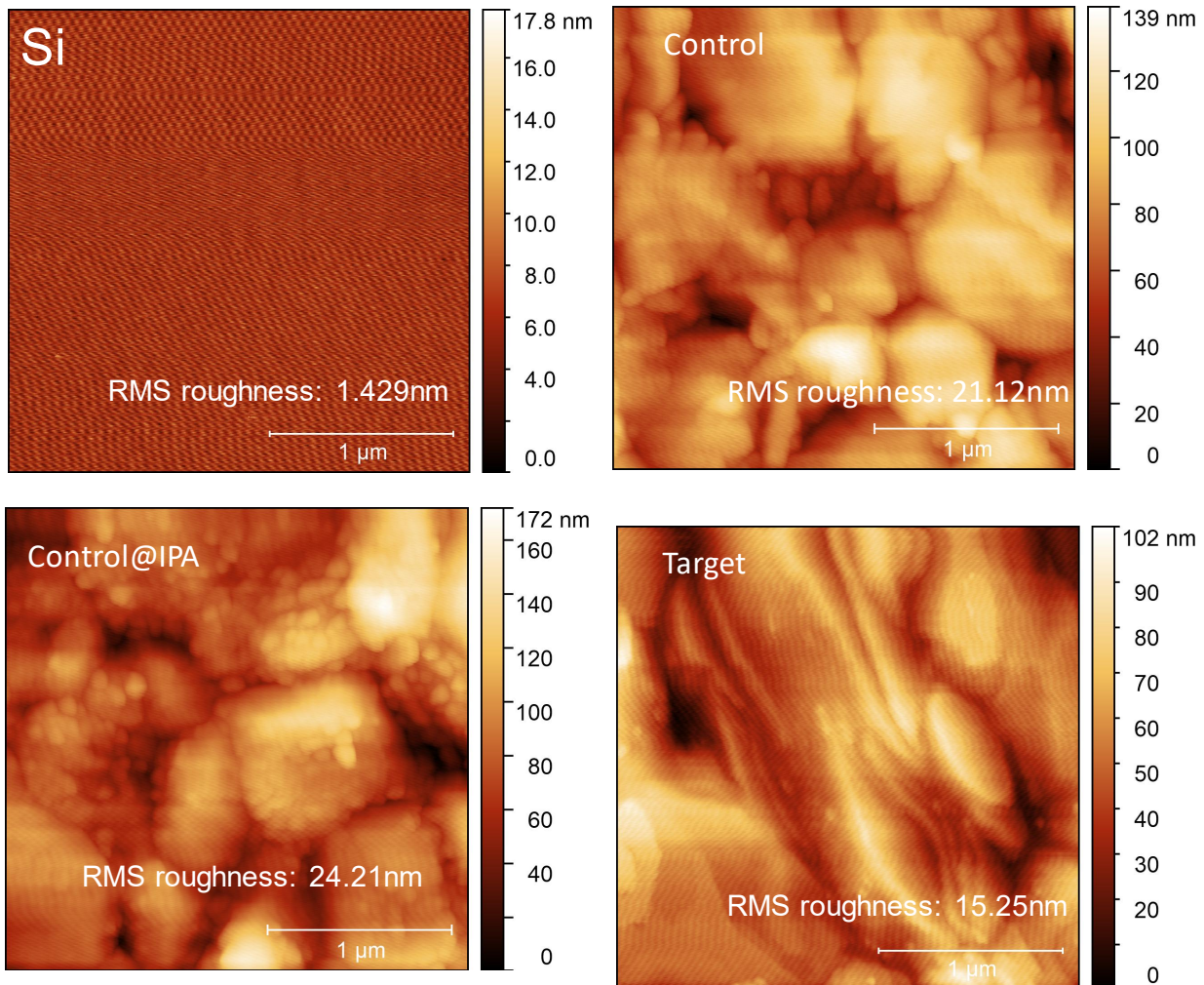


Figure S5. AFM image of silicon wafer(Si), Control, Control@IPA, and target samples.sample structure: Si/NiOx/SAM/Perovskite(w, w/o TPPO).Note The only difference between Control and Control@IPA is that Control@IPA was rinsed with IPA.

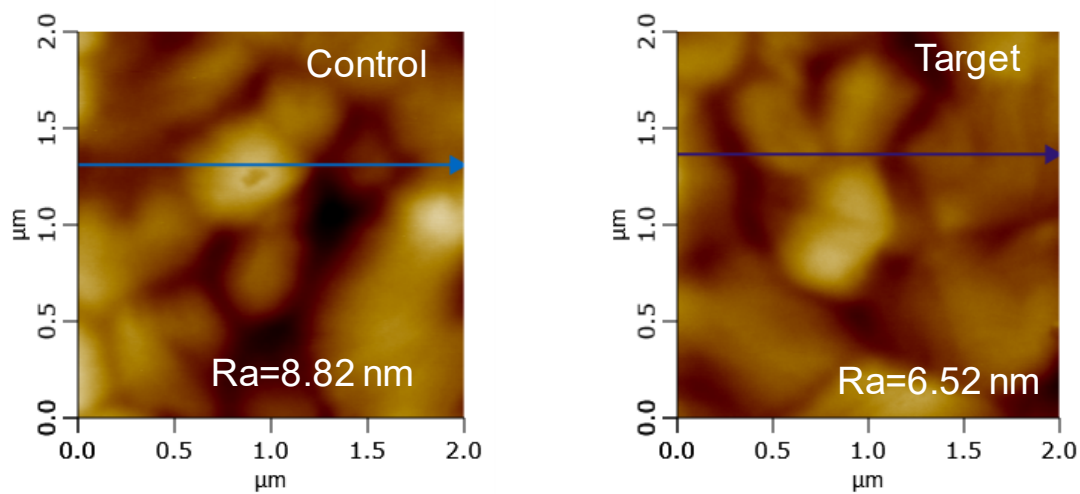


Figure S6. AFM image of control and target samples. sample architecture: Si/NiOx/SAM/Perovskite(w, w/o TPPO)/PCBM

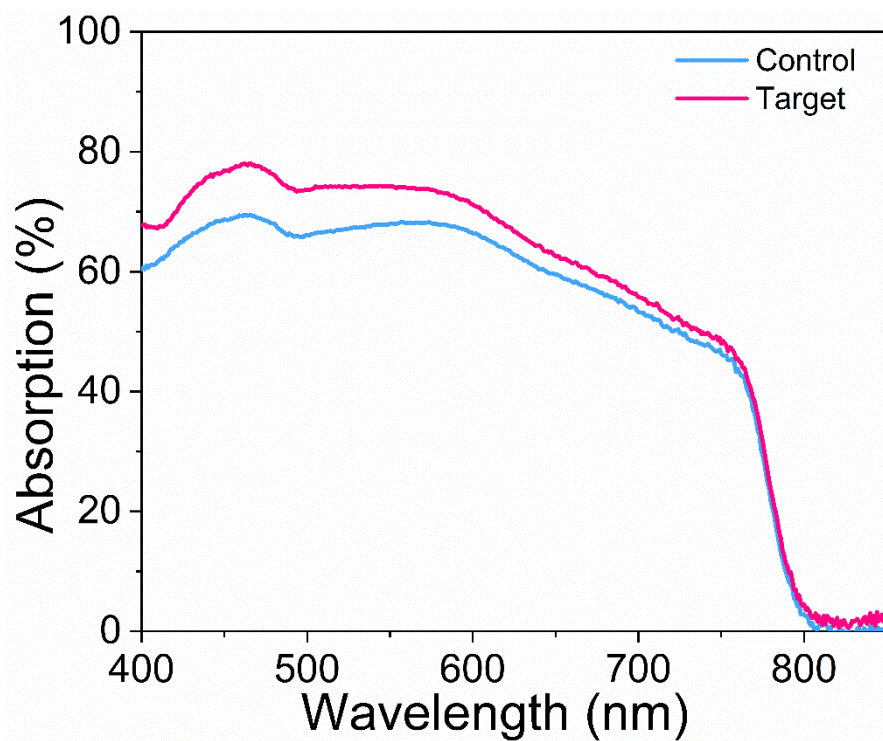


Figure S7. UV-Vis spectra of Control and Target sample.

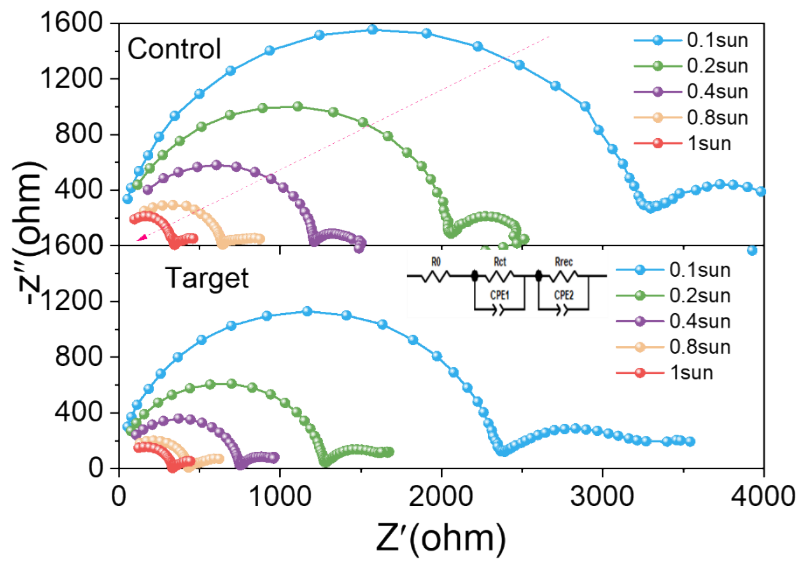


Figure S8 Mott–Schottky plots of PSCs based on control, target. Nyquist plots of PSCs devices based on control and perovskite with TPPO, The Nyquist plots of sample are measured at different light intensity

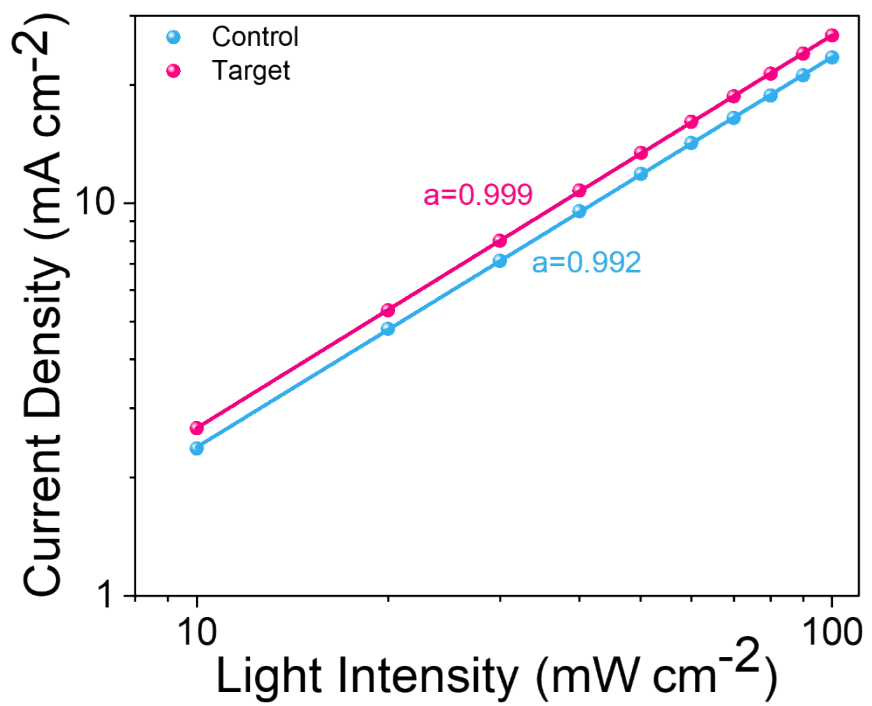


Figure S9 J_{sc} versus light intensity of Control and Target samples

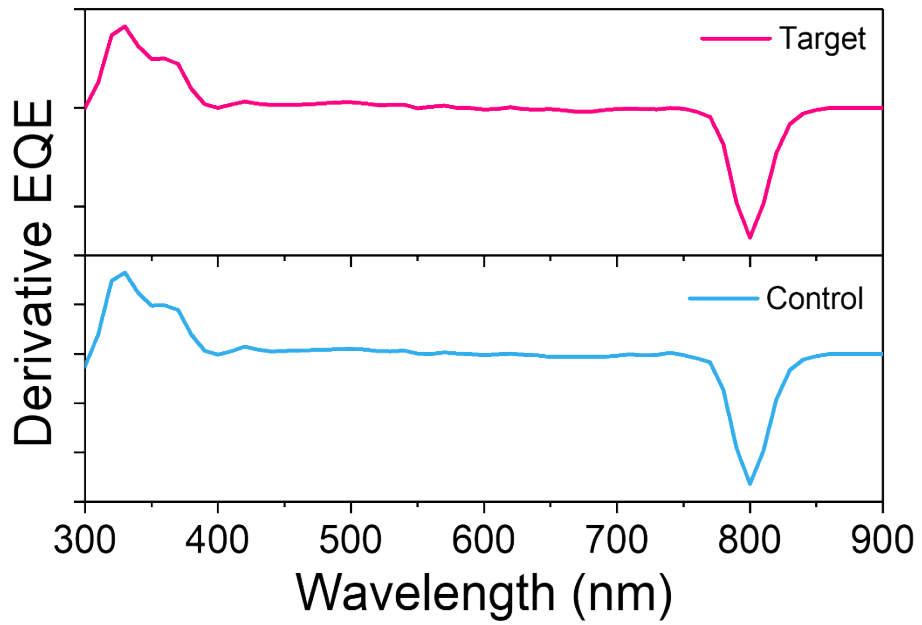


Figure S10 Eg, estimation obtained from the inflection point of the EQE spectra by locating the maximum point (λg) of the Gaussian-like derivate $\partial EQE / \partial \lambda$ ($1240 / 800 = 1.55$ eV).

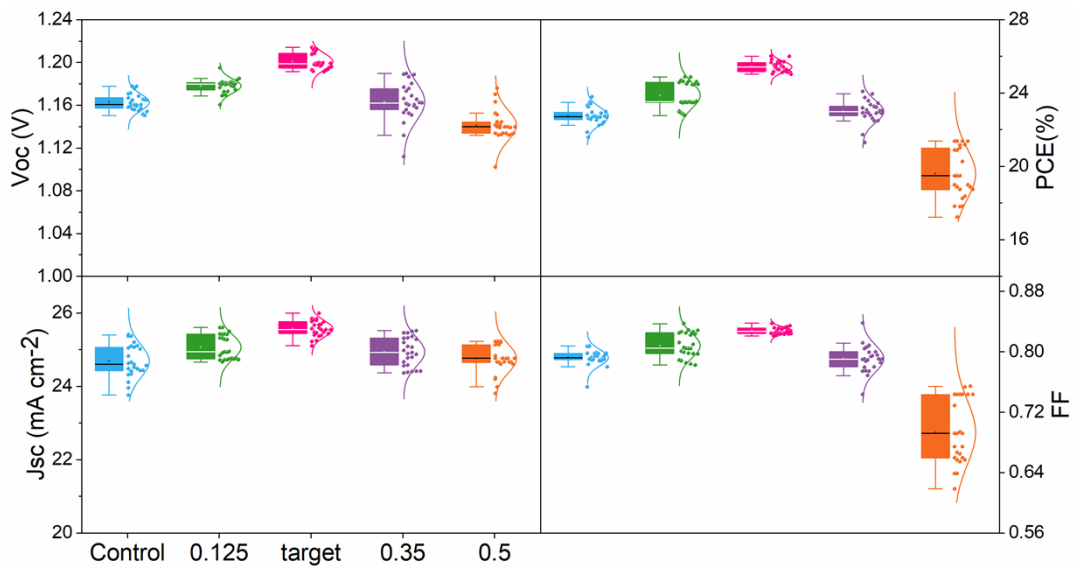


Figure S11 Statistics of key photovoltaic parameters (open-circuit voltage (V_{OC}), fill factor (FF), short-circuit current density (J_{SC}), PCE) obtained from the J - V characteristic of 25 control devices, and devices modified with different concentrations of TPPO (0.0, 0.125, 0.25, 0.35 and 0.5 mg ml^{-1}).

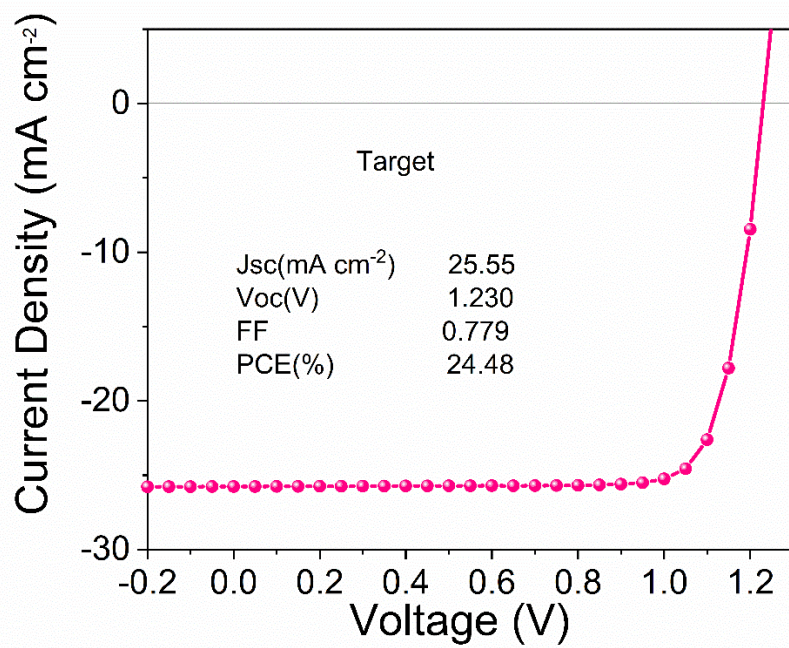


Figure S12 The J - V curve of some individual target PSC with a high V_{OC} of 1.23V (reverse scan).

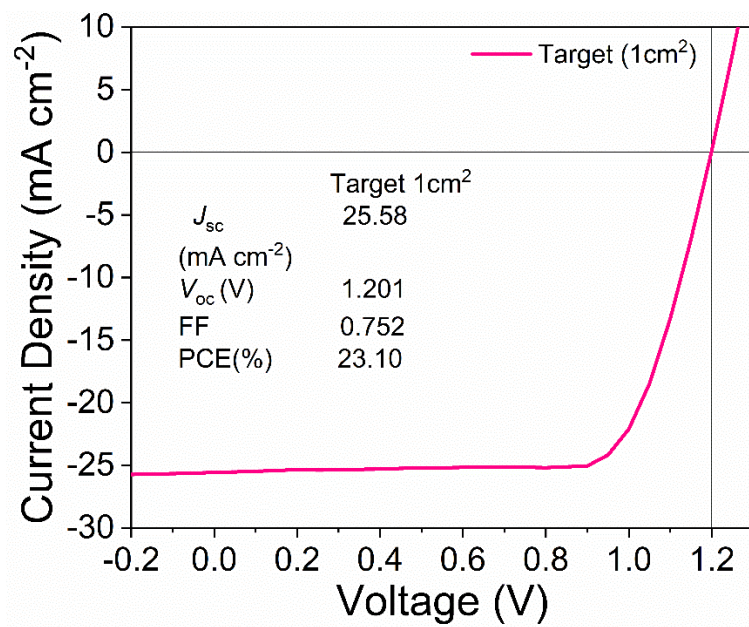


Figure S13 J - V curve of 1cm^2 -active layer.

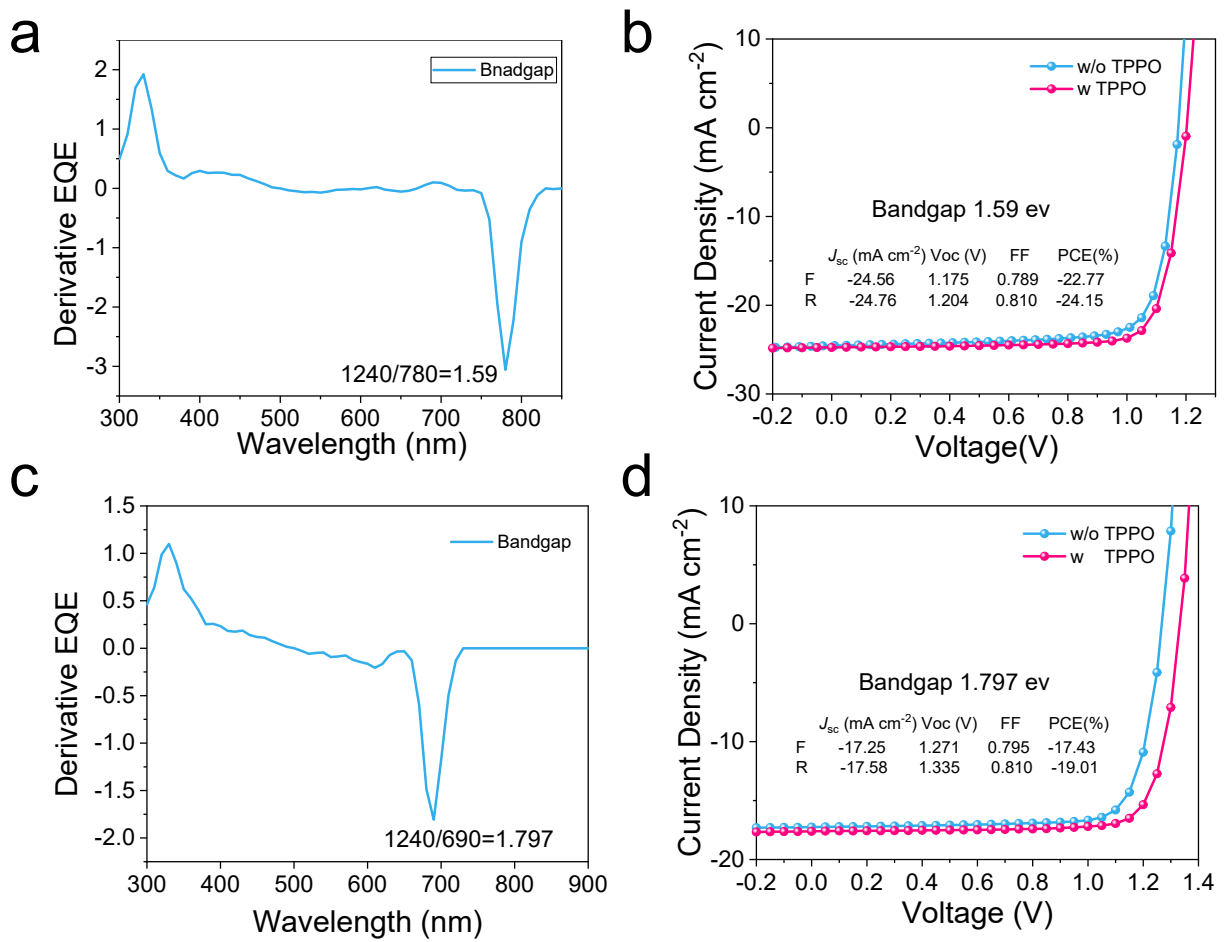


Figure S14 J-V curves of different band gaps with, without, TPPO modification (Reverse scan)

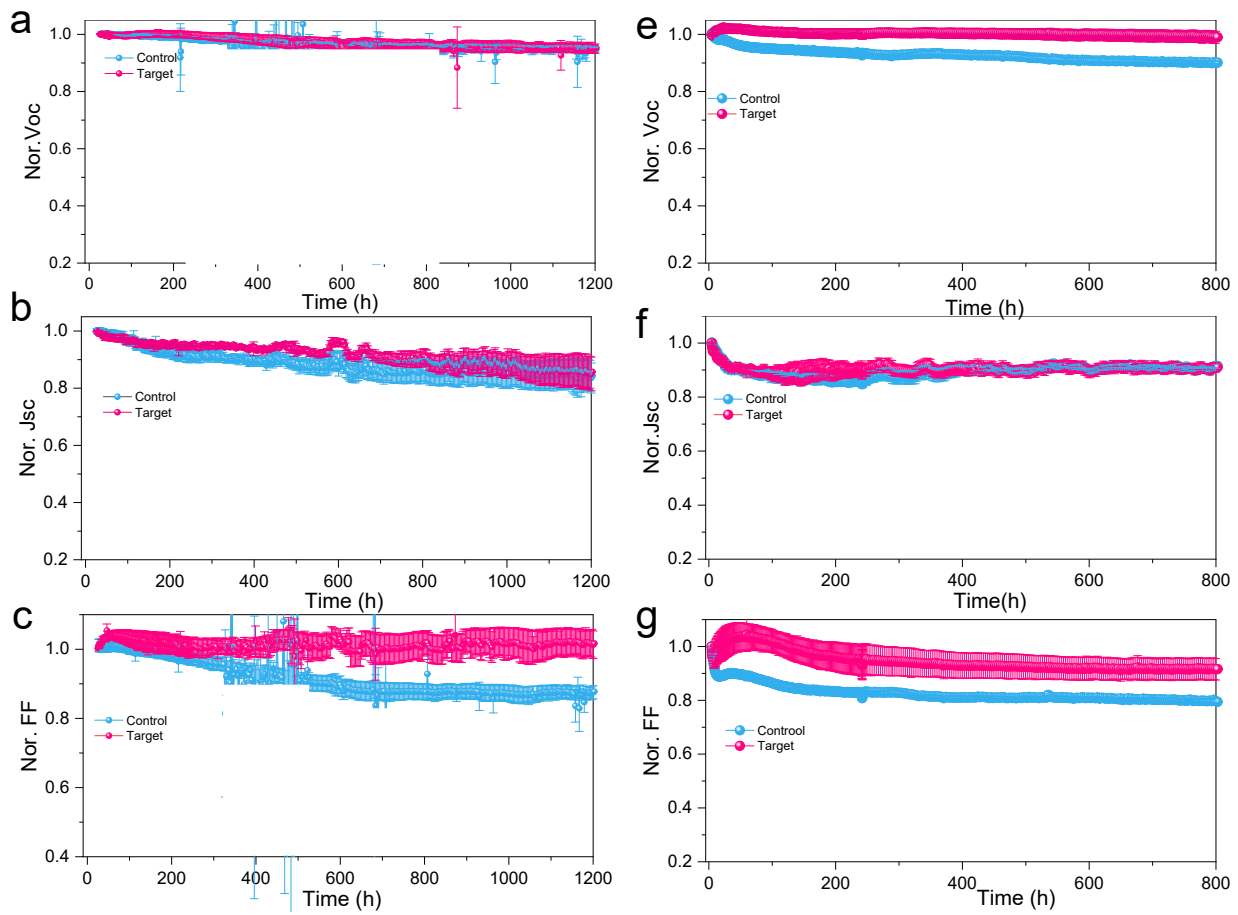


Figure S15 Long-term operational stability of device's J_{sc} , V_{oc} , FF under continuous output at MPP conditions (1 sun, LED lamps with ultraviolet filter; 65 °C (a-c) and 85 °C (e-g) in N₂-filled Chamber.

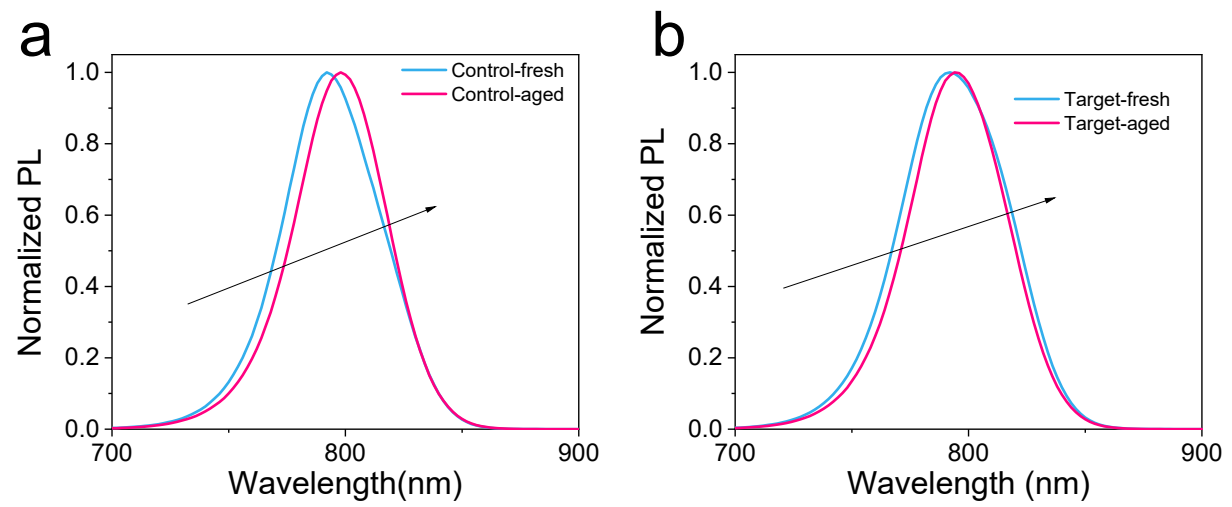


Figure S16 the PL evolution of control and target sample after 300 h under 1suns and 65 °C

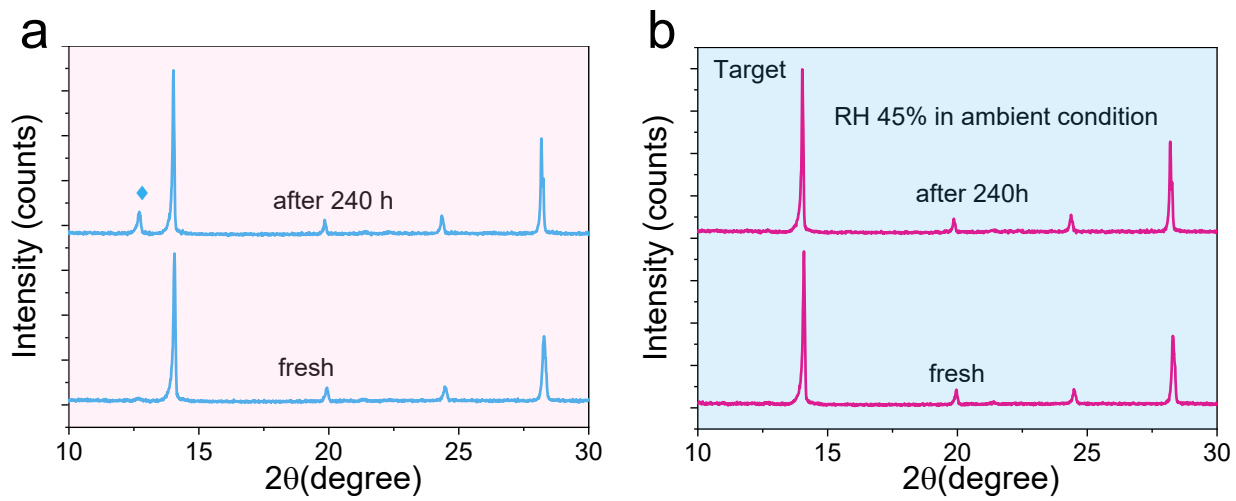


Figure S17 the evolution of XRD under ambient conditions without (a) and with (b) TPPO

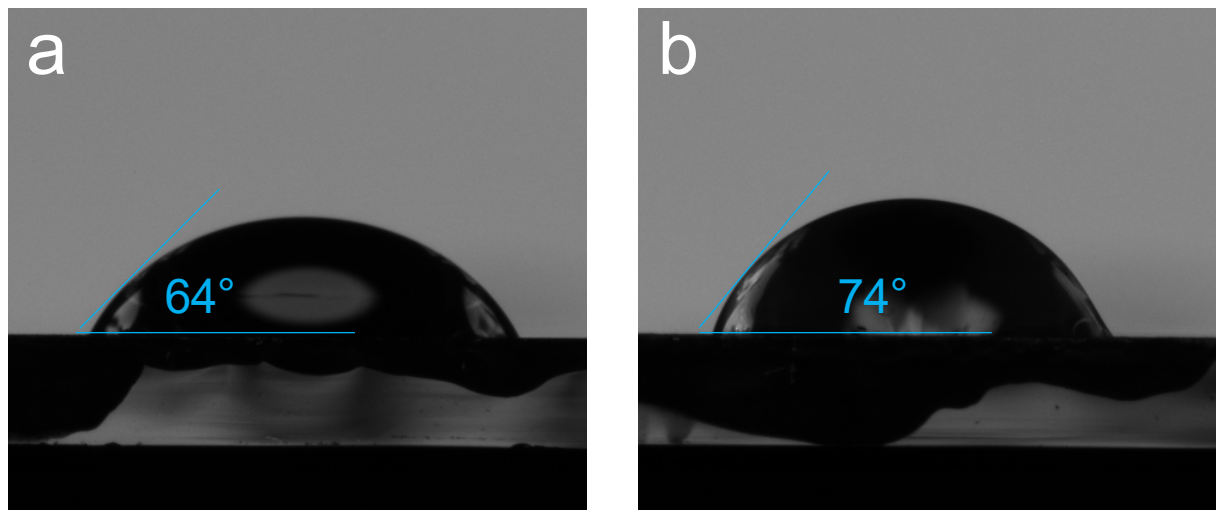


Figure S18 Water contact angle of the films processed without (a) and with TPPO-treated (b).

Table S1 Statistics on the application of TPPO in perovskite devices and LEDs

PeLEDs				
No	Title	EQE (%)	Journal	Summary
1	Distribution control enables efficient reduced-dimensional perovskite LEDs	25.6(2.5 times)	Nature 599, 594–598 (202, DOI: 10.1038/s41586-021-03997-z	TPPO regulates quantum well distribution and passivates defects, boosting efficiency and color purity in reduced-dimensional PeLEDs
2	Efficient all-thermally evaporated perovskite light-emitting diodes for active-matrix displays	16.4(2times)	Nature Photo. DOI: 10.1038/s41566-023-01177-1	The use of TPPO provides efficient all-thermal evaporated PeLED for active matrix displays
3	Phosphine oxide additives for perovskite light-emitting diodes and solar cells	Review	Chem, 2023, DOI: 10.1016/j.chempr.2023.01.002	A comprehensive review summarizing phosphine oxide ligands, including TPPO, with emphasis on their widespread use in PeLEDs.
4	Efficient Perovskite Light-Emitting Diodes by Buried Interface Modification with Triphenylphosphine Oxide	21.01(1.58times)	ACS Applied Materials & Interfaces, 2023, DOI: 10.1021/acsami.2c19123	TPPO was introduced at the buried interface to reduce interfacial defects, achieving an EQE of 21.01%.
5	Phosphine Oxide Additives for High-Brightness Inorganic Perovskite Light-Emitting Diodes	9.5(2.1times)	Advanced Optical Materials, 2021, DOI: 10.1002/adom.202101602	Study demonstrating enhanced luminance and stability of inorganic PeLEDs using TPPO additives.
6	Bilayer phosphine oxide	4.87(2 times)	Science Bulletin, 2023, DOI:	Use of bilayer phosphine oxide including

	modification toward efficient and large-area pure-blue perovskite quantum dot LEDs		10.1016/j.scib.2023.09.014	TPPO for performance enhancement in large-area blue QD PeLEDs.
7	Fluorine-modified passivator for efficient vacuum-deposited pure-red PeLEDs	12.6(640nm,6tim es)	Light: Science & Applications, 2025, DOI: 10.1038/s41377-025-01740-1	Study utilizing fluorinated TPPO analogs in red-emitting vacuum-deposited PeLEDs.
8	Trade-off between efficiency and stability in Mn ²⁺ -doped perovskite LEDs	14(4.7time)	Device, 2023, DOI: 10.1016/j.device.2023.100017	TPPO and similar phosphine oxide ligands were found effective for efficiency improvement.
9	Effect of Passivating Molecules and Antisolvents on Lifetime of Green Dion–Jacobson Perovskite Light-Emitting Diodes	12.42 (520nm,1.11time s)	ACS Applied Materials & Interfaces, 2023, DOI: 10.1021/acsami.3c02170	Study shows TPPO helps improve lifetime of quasi-2D PeLEDs.
10	Perovskite LEDs with an external quantum efficiency exceeding 25%		Nature Materials, 2022,	Comparative study of fluorinated and non-fluorinated phosphine oxides including TPPO.
11	A roadmap for the commercialization of perovskite light emitters		Nature Reviews Materials, 2022, DOI: 10.1038/s41578-022-00459-4	Review of commercialization strategies including surface treatments like TPPO.
12	The regulatory effect of triphenylphosphine oxide on	Review	Journal of Materials Chemistry C, 2021, DOI: 10.1039/D1TC01320C	TPPO functions as an interfacial modulator that enhances perovskite film crystallinity and

	perovskites for morphological and radiative improvement			improves its photoluminescence performance by effective surface passivation.
13	Exploring the Critical Factors Toward Spectrally Stable Mixed-Halide Blue Perovskite LEDs	11.5(477nm,1.82 time)	ChemPhotoChem,2024, DOI: 10.1002/cptc.202400019	TPPO effectively passivates surface defects and suppresses halide segregation, which stabilizes the emission spectrum and improves efficiency
14	Phosphonate/Phosphine Oxide Dyad Additive for Efficient and Spectrally Stable Blue Perovskite Light-Emitting Diodes	11(474nm,3.54time)	Angewandte Chemie,2022. DOI: 10.1002/ange.202117374	TPPO acts as a surface passivating agent that suppresses halide ion migration and non-radiative recombination, thereby enhancing the spectral stability and efficiency of blue perovskite LEDs.
15	Lewis Base Passivation of Quasi-2D Ruddlesden–Popper Perovskite for Order of Magnitude Photoluminescence Enhancement and Improved Stability	PL intensity (10 times)	ACS Applied Electronic Materials,2021, DOI: 10.1021/acsami.2c19123	TPPO functions as a strong Lewis base that passivates surface defects and suppresses halide ion migration, thereby significantly enhancing the efficiency and spectral stability of perovskite LEDs.
16.	Edge stabilization in reduced-dimensional perovskites" was published in Nature Communications,	14%(517nm,5.6time)	Nature Communications, 2020, 11, 170, DOI: 10.1021/acsami.2c19123	TPPO passivates Pb ²⁺ defects and suppresses non-radiative recombination, boosting efficiency and spectral stability in perovskite LEDs
17	A bilateral interfacial passivation strategy promoting efficiency and stability of perovskite quantum dot light-emitting diodes	18.7(520nm, 2.43times)	Nature Communications,11,2020, DOI: 10.1038/s41467-020-17633-3	TPPO passivates interfacial defects and suppresses non-radiative recombination, thereby enhancing the efficiency, spectral stability, and operational lifetime of perovskite LEDs

18.	All-Thermally Evaporated Blue Perovskite Light-Emitting Diodes for Active Matrix Displays	2.47(475nm)	Small Methods, 2024., DOI:10.1002/smtd.202300712	TPPO passivates interfacial defects and inhibits ion migration, thereby enhancing efficiency and spectral stability in perovskite LEDs.
19.	Additives in Halide Perovskite for Blue-Light-Emitting Diodes: Passivating Agents or Crystallization Modulators?	7.8(480nm,2.3times)	ACS Energy Letters, 2021, DOI:10.1021/acsenergylett.1c02232	TPPO passivates defects and modulates crystallization, enhancing efficiency and spectral stability in perovskite LEDs.
20	Multi-site anchoring lead-halide octahedral by benzylphosphonic acid to regulate phase distribution for efficient PeLEDs	20.6(514nm, 2.6times)	Nano Research ,2024, DOI:10.1007/s12274-024-6914-9	Benzylphosphonic acid (BPA) enhances perovskite LED performance by anchoring lead-halide octahedra to regulate phase distribution and passivate defects, resulting in improved efficiency and stability
21	All-Thermally Evaporated Perovskite LEDs Toward High-Resolution Active-Matrix Displays		Matter.2023, DOI: 10.1016/j.matt.2023.05.041	These results highlight the potential of all-thermally evaporated processes for the scalable production of high-performance blue PeLEDs suitable for display application

Perovskite Solar cells					
Architecture	Jsc (mA cm ⁻²)	Voc(V)	FF(%)	PCE(%)	Reference
n-i-p	23.7	1.131	79	21.2	Advanced Materials, 2020, 32(23): 1907396.
p-i-n, MAPbI₃	21.32	0.94	72	14.9	Optical Materials, 2022, 127: 112264
n-i-p CsPbBr ₃	7.87	1.28	72	7.28	ACS Applied Materials & Interfaces, 2024, 16(50): 69410-69417
n-i-p MAFACs	23.9	1.15	73.5	20.3	Chemical Engineering Journal, 2020, 396: 125010

n-i-p FAMA- 4FTPPO	25.25	1.13	79.3	22.63	Applied Physics Letters, 2025, 126(2)
p-i-n MA-free	25.57	1.214	83.8	26.01	This Work

Table S2 Fitting all parameters of the TRPL spectra. Bimolecular (k_B), trapping (k_T), and

Samples	Intensity of suns	$R_{ct}(\text{ohm})$	$R_{rec}(\text{ohm})$
Control	1	340	124.4
	0.8	601	152
	0.4	1178	213.9
	0.2	2024	417
	0.1	3199	905
	1	309.7	110
Target	0.8	406.3	150
	0.4	725	183.1
	0.2	1246	328.4
	0.1	2317	714.3

detrapping (k_D), accompanied by trap state density (N_T) and doping concentration (p_0) extracted from 'Bimolecular-Trapping-Detrapping Model' in 'PEARS (<https://pears-tool.herokuapp.com/>)'.

Samples	$k_B \times 10^{-21}$ (cm ³ /ns)	$k_T \times 10^{-15}$ (cm ³ /ns)	$K_D \times 10^{-19}$ (cm ³ /ns)	$N_T \times 10^{13}$ (cm ³)	$P_0 \times 10^{15}$ (cm ³)
Control	7.57	1.49	9.7	112	6.5
Target	2.07	1.97	113	4	1.4

Table S3 Fitting parameters of the TRPL spectra for the control and TPPO-modified films.

Samples	Photoexcited carrier concentrations (10^{16}cm^{-3})	Trapping (%)	Bimolecular (%)	Detrapping (%)
Control	4.40	69.77	9.20	21.03
	8.34	64.51	15.54	19.95
	17.9	58.19	25.61	16.20
	4.40	46.58	12.39	41.03
Target	8.34	41.82	20.83	37.35
	17.9	34.34	35.07	30.59

Table S4 EIS parameters of the PSCs under different intensity of suns

Table S5 Performance parameters of p-i-n solar cells with ~ 1.55 eV bandgap

Devices Structure	Perovskite composition	Voc deficit s	Voc [V]	Jsc [mA cm ⁻²]	FF [%]	PCE [%]	Ref.
ITO/ NiO _x /Me-4PACz /PVK/C ₆₀ /BCP/Bi/Ag	FA _{0.95} Cs _{0.05} PbI ₃	0.338	1.192	26.47	84.11	26.54	⁴
p-i-n (1.52) FTO/MeO-2PACz/PVK/C ₆₀ /BCP/Cu	FAPbI ₃	0.4	1.12	25.5	82	24.1	⁵
p-i-n (1.53) FTO/MeO-2PACz/PVK/C ₆₀ /BCP/Ag	(FAPbI ₃) _{0.95} (MAPbBr ₃) _{0.05}	0.35	1.18	25.9	85.4	26	⁶
p-i-n (1.52) ITO/SAM/PVK/C ₆₀ /BCP/Au	FA _{0.72} Cs _{0.1} MA _{0.18} PbI ₃	0.35	1.17	25.4	84	25.1	⁷
p-i-n (1.55) ITO/PTAA/PVK/Fc-derived/C ₆₀ /BCP/Ag	Cs _{0.05} (FA _{0.98} MA _{0.02}) _{0.95} Pb(I _{0.98} Br _{0.02}) ₃	0.356	1.194	25.93	84.24	26.08	⁸
p-i-n (1.55) ITO/NiOX/MeO- PhPACz/PVK/PI/C ₆₀ /BCP/Cu	Cs _{0.05} MA _{0.1} FA _{0.85} PbI ₃	0.361	1.189	25.37	86.79	26.17	⁹
p-i-n (1.55) ITO/NiOX/PTAA/Al ₂ O ₃ /PVK/PCBM/BCP/A g	FA _{0.95} Cs _{0.05} PbI ₃	0.346	1.184	26.11	84.2	26.03	¹⁰
p-i-n (1.55) FTO/2PACz/2D/3D-PVK/2D/C ₆₀ /BCP/Cu	Cs _{0.01} (FA _{0.98} MA _{0.02}) _{0.95} PbI ₃	0.372	1.178	25.67	86.47	26.15	¹¹
p-i-n (1.53) ITO/2PACz/2D/PVK/2D/C ₆₀ /SnO ₂ /IZO/Cu	Cs _{0.025} MA _{0.075} FA _{0.90} PbI ₃	0.34	1.19	24.94	85.9	25.63	¹²
p-i-n (1.53) ITO/2PACz/PVK/2D/C ₆₀ /SnO ₂ /IZO/Cu	Cs _{0.01} (FA _{0.97} MA _{0.03}) _{0.99} Pb(I _{0.97} Br _{0.03}) ₃	0.345	1.185	25.41	84.6	25.42	¹³
p-i-n (1.54) FTO/MeO-2PACz/PVK/PCBM/YbOx/Cu	Rb _{0.05} Cs _{0.05} MA _{0.05} FA _{0.85} Pb(I _{0.95} Br _{0.05}) ₃	0.38	1.16	26.1	83	25.2	¹⁴
p-i-n (1.55) ITO/NiOx/PTAA/Al ₂ O ₃ /PVK/PCBM/BCP/Ag	Cs _{0.05} FA _{0.95} PbI ₃	0.38	1.17	26.2	82.2	25.12	¹⁵
p-i-n (1.53) ITO/p-PY/PVK/PCBM/BCP/Ag	FA _{0.98} Cs _{0.02} PbI ₃	0.363	1.167	25.75	81.5	24.5	¹⁶
p-i-n (1.544) ITO/DMAcPA/PVK/PCBM/BCP/Ag	Cs _{0.055} (FA _{0.95} MA _{0.05}) _{0.945} Pb(I _{0.9} Br _{0.1}) ₃	0.355	1.189	25.69	84.91	25.86 (certi fied 25.39)	¹⁷
p-i-n (1.563) ITO/MeO-4PACz@PVK/C ₆₀ /BCP/Ag	Cs _{0.05} (FA _{0.95} MA _{0.05}) _{0.95} Pb(I _{0.95} Br _{0.05}) ₃	0.362	1.201	24.8	84.5	25.16	¹⁸
p-i-n (1.55) ITO/ DC-PA /PVK/C ₆₀ /BCP/Ag	Cs _{0.06} MA _{0.14} FA _{0.80} PbI ₃	0.36	1.19	24.55	84.78	24.8 (certi fied2 4.5)	¹⁹
p-i-n (1.53) FTO/NiOx/Me-4PACz/(with or without) DPPP/PVK/PEAI/C ₆₀ /SnO ₂ /Ag	FA _{0.95} Cs _{0.05} PbI ₃ +0.6mol% MAPbBr ₃	0.37	1.16	25.73	82.5	24.5	²⁰
p-i-n (1.55) ITO/PTAA/PVK/C ₆₀ /BCP/Ag	Cs _{0.05} (FA _{0.98} MA _{0.02}) _{0.95} Pb(I _{0.98} Br _{0.02}) ₃	0.366	1.184	25.68	82.32	25	²¹
p-i-n (1.56) ITO/MeO-4PACz@PVK/C ₆₀ /BCP/Ag	Cs _{0.05} (FA _{0.98} MA _{0.02}) _{0.95} Pb(I _{0.98} Br _{0.02}) ₃	0.37	1.19	24.78	83.07	24.5	²²
p-i-n (1.55) ITO/MeO-2PACz/PVK/PCBM/BCP/Ag	Cs _{0.05} (FA _{0.98} MA _{0.02}) _{0.95} Pb(I _{0.98} Br _{0.02}) ₃	0.373	1.177	24.8	84.3	24.6	²³
p-i-n (1.563) ITO/MeO-4PACz@PVK/C ₆₀ /BCP/Ag	Cs _{0.05} (FA _{0.95} MA _{0.05}) _{0.95} Pb(I _{0.95} Br _{0.05}) ₃	0.355	1.208	25.08	84.37	25.56	²⁴
p-i-n (1.56) ITO/PTAA/PVK/C ₆₀ /BCP/Cu	Cs _{0.05} (FA _{0.92} MA _{0.08}) _{0.95} Pb(I _{0.92} Br _{0.08}) ₃	0.39	1.17	24.1	81.6	23	²⁵
p-i-n (1.55) ITO/PTAA-P1/PVK/C ₆₀ /BCP/Ag	Cs _{0.05} (FA _{0.92} MA _{0.08}) _{0.95} Pb(I _{0.92} Br _{0.08}) ₃	0.38	1.17	25.50	83.28	24.89	²⁶
p-i-n (1.55) ITO/2PACZ/PVK/C ₆₀ /BCP/Ag	Cs _{0.03} (FA _{0.90} MA _{0.10}) _{0.97} PbI ₃	0.35	1.20	24.7	82	24.3	²⁷

p-i-n (1.55) ITO/Me-4PACz@MPA/PVK/PCBM/BCP/Ag	Cs _{0.1} FA _{0.90} PbI ₃	0.336	1.214	25.57	83.8	26.01	This work
p-i-n (1.55) ITO/Me-4PACz@MPA/PVK/PCBM/BCP/Ag	Cs _{0.1} FA _{0.90} PbI ₃ (active layer 1cm ²)	0.320	1.230	25.55	78	24.51	

Table S6. PV Parameters of the Best-Performing Perovskite Solar Cells

1. Z. Peng, J. Tian, K. Zhang, A. These, Z. Xie, Y. Zhao, A. Osvet, F. Guo, L. Lüer, N. Li and

Devices	Scan direction	V_{OC} (V)	FF (%)	J_{SC} (mA cm $^{-2}$)	PCE (%)	Hysteresis Index
Control	Forward	1.155	78.9	25.40	23.15	0.027
	Reverse	1.161	80.8	25.30	23.79	
Target	Forward	1.195	83.4	25.61	25.52	0.019
	Reverse	1.214	83.8	25.57	26.01	

C. J. Brabec, *ACS Energy Letters*, 2023, **8**, 2077-2085.

2. J. Tian, K. Zhang, Z. Xie, Z. Peng, J. Zhang, A. Osvet, L. Lüer, T. Kirchartz, U. Rau, N. Li and C. J. Brabec, *ACS Energy Letters*, 2022, **7**, 4071-4080.
3. K. Zhang, A. Späth, O. Almora, V. M. Le Corre, J. Wortmann, J. Zhang, Z. Xie, A. Barabash, M. S. Hammer, T. Heumüller, J. Min, R. Fink, L. Lüer, N. Li and C. J. Brabec, *ACS Energy Letters*, 2022, **7**, 3235-3243.
4. S. Liu, J. Li, W. Xiao, R. Chen, Z. Sun, Y. Zhang, X. Lei, S. Hu, M. Kober-Czerny, J. Wang, F. Ren, Q. Zhou, H. Raza, Y. Gao, Y. Ji, S. Li, H. Li, L. Qiu, W. Huang, Y. Zhao, B. Xu, Z. Liu, H. J. Snaith, N.-G. Park and W. Chen, *Nature*, 2024, DOI: 10.1038/s41586-024-07723-3.
5. S. Sidhik, I. Metcalf, W. Li, T. Kodalle, C. J. Dolan, M. Khalili, J. Hou, F. Mandani, A. Torma, H. Zhang, R. Garai, J. Persaud, A. Marciel, I. A. Muro Puente, G. N. M. Reddy, A. Balvanz, M. A. Alam, C. Katan, E. Tsai, D. Ginger, D. P. Fenning, M. G. Kanatzidis, C. M. Sutter-Fella, J. Even and A. D. Mohite, *Science*, 2024, **384**, 1227-1235.
6. T. Duan, S. You, M. Chen, W. Yu, Y. Li, P. Guo, J. J. Berry, J. M. Luther, K. Zhu and Y. Zhou, *Science*, 2024, **384**, 878-884.
7. W.-T. Wang, P. Holzhey, N. Zhou, Q. Zhang, S. Zhou, E. A. Duijnstee, K. J. Rietwyk, J.-Y. Lin, Y. Mu and Y. J. N. Zhang, *Nature*, 2024, 1-2.
8. B. Li, D. Gao, S. A. Sheppard, W. D. J. Tremlett, Q. Liu, Z. Li, A. J. P. White, R. K. Brown, X. Sun, J. Gong, S. Li, S. Zhang, X. Wu, D. Zhao, C. Zhang, Y. Wang, X. C. Zeng, Z. Zhu and N. J. Long, *Journal of the American Chemical Society*, 2024, **146**, 13391-13398.
9. G. Qu, S. Cai, Y. Qiao, D. Wang, S. Gong, D. Khan, Y. Wang, K. Jiang, Q. Chen and L. J. J. Zhang, *Joule*, 2024.
10. C. Gong, H. Li, H. Wang, C. Zhang, Q. Zhuang, A. Wang, Z. Xu, W. Cai, R. Li, X. Li and Z. Zang, *Nature Communications*, 2024, **15**, 4922.
11. Y. Zheng, Y. Li, R. Zhuang, X. Wu, C. Tian, A. Sun, C. Chen, Y. Guo, Y. Hua, K. J. E.

- Meng and E. Science, 2024, **17**, 1153-1162.
- 12. R. Azmi, D. S. Utomo, B. Vishal, S. Zhumagali, P. Dally, A. M. Risqi, A. Prasetio, E. Ugur, F. Cao, I. F. Imran, A. A. Said, A. R. Pininti, A. S. Subbiah, E. Aydin, C. Xiao, S. I. Seok and S. De Wolf, *Nature*, 2024, **628**, 93-98.
 - 13. H. Meng, K. Mao, F. Cai, K. Zhang, S. Yuan, T. Li, F. Cao, Z. Su, Z. Zhu, X. Feng, W. Peng, J. Xu, Y. Gao, W. Chen, C. Xiao, X. Wu, M. D. McGehee and J. Xu, *Nature Energy*, 2024, DOI: 10.1038/s41560-024-01471-4.
 - 14. P. Chen, Y. Xiao, J. Hu, S. Li, D. Luo, R. Su, P. Caprioglio, P. Kaienburg, X. Jia, N. Chen, J. Wu, Y. Sui, P. Tang, H. Yan, T. Huang, M. Yu, Q. Li, L. Zhao, C.-H. Hou, Y.-W. You, J.-J. Shyue, D. Wang, X. Li, Q. Zhao, Q. Gong, Z.-H. Lu, H. J. Snaith and R. Zhu, *Nature*, 2024, **625**, 516-522.
 - 15. H. Li, C. Zhang, C. Gong, D. Zhang, H. Zhang, Q. Zhuang, X. Yu, S. Gong, X. Chen, J. Yang, X. Li, R. Li, J. Li, J. Zhou, H. Yang, Q. Lin, J. Chu, M. Grätzel, J. Chen and Z. Zang, *Nature Energy*, 2023, **8**, 946-955.
 - 16. R. Chen, J. Wang, Z. Liu, F. Ren, S. Liu, J. Zhou, H. Wang, X. Meng, Z. Zhang, X. Guan, W. Liang, P. A. Troshin, Y. Qi, L. Han and W. Chen, *Nature Energy*, 2023, **8**, 839-849.
 - 17. Q. Tan, Z. Li, G. Luo, X. Zhang, B. Che, G. Chen, H. Gao, D. He, G. Ma, J. Wang, J. Xiu, H. Yi, T. Chen and Z. He, *Nature*, 2023, **620**, 545-551.
 - 18. S. Zhang, F. Ye, X. Wang, R. Chen, H. Zhang, L. Zhan, X. Jiang, Y. Li, X. Ji, S. Liu, M. Yu, F. Yu, Y. Zhang, R. Wu, Z. Liu, Z. Ning, D. Neher, L. Han, Y. Lin, H. Tian, W. Chen, M. Stolterfoht, L. Zhang, W.-H. Zhu and Y. Wu, *Science*, 2023, **380**, 404-409.
 - 19. F. Li, X. Deng, Z. Shi, S. Wu, Z. Zeng, D. Wang, Y. Li, F. Qi, Z. Zhang, Z. Yang, S.-H. Jang, F. R. Lin, S. W. Tsang, X.-K. Chen and A. K. Y. Jen, *Nature Photonics*, 2023, **17**, 478-484.
 - 20. C. Li, X. Wang, E. Bi, F. Jiang, S. M. Park, Y. Li, L. Chen, Z. Wang, L. Zeng, H. Chen, Y. Liu, C. R. Grice, A. Abudulimu, J. Chung, Y. Xian, T. Zhu, H. Lai, B. Chen, R. J. Ellingson, F. Fu, D. S. Ginger, Z. Song, E. H. Sargent and Y. Yan, *Science*, 2023, **379**, 690-694.
 - 21. Z. Li, B. Li, X. Wu, S. A. Sheppard, S. Zhang, D. Gao, N. J. Long and Z. Zhu, *Science*, 2022, **376**, 416-420.
 - 22. X. Zheng, Z. Li, Y. Zhang, M. Chen, T. Liu, C. Xiao, D. Gao, J. B. Patel, D. Kuciauskas, A. Magomedov, R. A. Scheidt, X. Wang, S. P. Harvey, Z. Dai, C. Zhang, D. Morales, H. Pruett, B. M. Wieliczka, A. R. Kirmani, N. P. Padture, K. R. Graham, Y. Yan, M. K. Nazeeruddin, M. D. McGehee, Z. Zhu and J. M. Luther, *Nature Energy*, 2023, **8**, 462-472.
 - 23. G. Li, Z. Su, L. Canil, D. Hughes, M. H. Aldamasy, J. Dagar, S. Trofimov, L. Wang, W. Zuo, J. J. Jerónimo-Rendon, M. M. Byranvand, C. Wang, R. Zhu, Z. Zhang, F. Yang, G. Nasti, B. Naydenov, W. C. Tsoi, Z. Li, X. Gao, Z. Wang, Y. Jia, E. Unger, M. Saliba, M. Li and A. Abate, *Science*, 2023, **379**, 399-403.
 - 24. W. Peng, K. Mao, F. Cai, H. Meng, Z. Zhu, T. Li, S. Yuan, Z. Xu, X. Feng, J. Xu, M. D.

- McGehee and J. Xu, *Science*, 2023, **379**, 683-690.
- 25. X. Zheng, Y. Hou, C. Bao, J. Yin, F. Yuan, Z. Huang, K. Song, J. Liu, J. Troughton, N. Gasparini, C. Zhou, Y. Lin, D.-J. Xue, B. Chen, A. K. Johnston, N. Wei, M. N. Hedhili, M. Wei, A. Y. Alsalloum, P. Maity, B. Turedi, C. Yang, D. Baran, T. D. Anthopoulos, Y. Han, Z.-H. Lu, O. F. Mohammed, F. Gao, E. H. Sargent and O. M. Bakr, *Nature Energy*, 2020, **5**, 131-140.
 - 26. X. Wu, D. Gao, X. Sun, S. Zhang, Q. Wang, B. Li, Z. Li, M. Qin, X. Jiang, C. Zhang, Z. Li, X. Lu, N. Li, S. Xiao, X. Zhong, S. Yang, Z. a. Li and Z. Zhu, *Advanced Materials*, 2023, **35**, 2208431.
 - 27. R. Azmi, E. Ugur, A. Seitkhan, F. Aljamaan, A. S. Subbiah, J. Liu, G. T. Harrison, M. I. Nugraha, M. K. Eswaran, M. Babics, Y. Chen, F. Xu, T. G. Allen, A. u. Rehman, C.-L. Wang, T. D. Anthopoulos, U. Schwingenschlögl, M. De Bastiani, E. Aydin and S. De Wolf, *Science*, 2022, **376**, 73-77.